

# HYPIC: Accelerating Hybrid-Attention LLM Serving with Position-Independent Caching

Yifei Liu\*  
Xiaohongshu Inc.  
liuyifei5@xiaohongshu.com

Juntong Wu\*  
Peking University  
wujt@stu.pku.edu.cn

Yang Liu  
Shanghai Jiao Tong University  
liuyang370@sjtu.edu.cn

Junhao Hu†  
Peking University  
junhao@stu.pku.edu.cn

Minghao Li  
Xiaohongshu Inc.  
leimuchen@xiaohongshu.com

Xiaoxu Chen  
Xiaohongshu Inc.  
chenxiaoxu@xiaohongshu.com

Weihang Chen  
Xiaohongshu Inc.  
chenjinzhi@xiaohongshu.com

## Abstract

In retrieval augmented generation (RAG) and agentic LLM serving, prompts are assembled from independent segments into long contexts, making the prefill stage dominate the per-request computation cost. To this cost, two directions have emerged in parallel: position-independent caching (PIC) admits KV reuse for non-contiguous segments shared across different requests, while hybrid-attention models reduce computation complexity by replacing most full-attention layers with linear attention. Although both directions accelerate LLM serving independently, they cannot coexist: applying PIC to hybrid-attention models breaks down because per-token KV-cache reuse primitives do not transfer to the per-request recurrent state.

In this work, we present HYPIC, the first serving system for hybrid-attention LLMs with position-independent caching. For linear-attention layers, we identify the segment-cumulative transition operator as the missing algebraic primitive, and cache it alongside each segment’s zero-start end-state, enabling near-exact and constant-time state composition of independently cached segments. For the remaining full-attention layers, existing PIC methods also fail as linear layers do not expose the per-token hidden states for selective recomputation. We show that the most significant attention deviation concentrates at segment boundaries, so recomputing only a small seam window at each boundary suffices to restore cross-segment lookback. Finally, HYPIC exploits segment-level self-containment to parallelize cache-miss prefill across instances, turning long cold requests—a major tail-latency contributor under both prefix caching and prior PIC—into an accelerable workload. Evaluated across four hybrid-attention models and five workloads, HYPIC reduces time-to-first-token (TTFT) by 2.45× on average and improves peak throughput by up to 2.0× over existing systems, while staying within 3.3 points of full-recompute accuracy.

\*Equal contribution.

†Corresponding author.

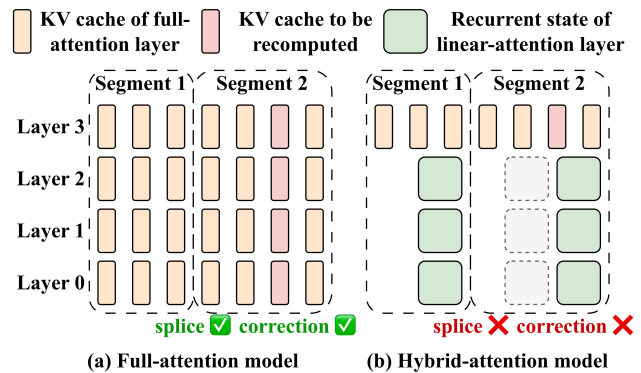


**Figure 1.** Existing PIC methods reuse per-token KV cache in full-attention models via *splice* and *correction* (left); on hybrid stacks, both primitives fail because linear-attention layers expose only a per-request recurrent state, with no per-token handle (right).

## 1 Introduction

Large language model (LLM) serving is shifting from single-turn chat toward retrieval-augmented question answering [11, 15, 34, 47], multi-document summarization [2, 7, 9], and long-horizon agents [14]. These workloads pull independent text segments (e.g., skills, memory files, etc.) from local or remote sources and embed them into a fixed prompt template, assembling contexts of tens to hundreds of thousands of tokens [2, 51]. At these lengths, prefill dominates the per-request compute bill and becomes one of the most prominent serving expenses for providers [36, 37]. Worse, on a cache miss, long cold requests push time-to-first-token (TTFT) into the multi-second tail, directly hurting interactive user experience [1, 26, 27, 54].

To reduce this cost, a growing body of work proposes *position-independent caching* (PIC) [12, 22–24, 37, 38, 40, 48, 49]. Unlike strict-prefix KV reuse, PIC caches each semantically independent segment once and allows it to be spliced

behind arbitrary prefixes, exactly matching how RAG and agentic prompts are assembled. All existing PIC systems are built on the same two primitives—*splice* along the token axis and *correction* to repair cross-segment context—both operating on per-token KV cache (Fig. 1, left).

In parallel, model architectures are also shifting. *Linear attention* [6, 18, 28, 32, 43–45] cuts the quadratic attention complexity to linear and compresses an unbounded KV history into a fixed-size recurrent state. Rather than replacing attention entirely, production models such as MiniMax-M1 [4], Qwen3.5 [29], Kimi-Linear [18], and Ring-2.5 [33] linearize the majority of layers ( $\geq 75\%$ ) while retaining a small fraction of full-attention layers, forming a *hybrid* stack that is now a mainstream design.

However, these two trends collide: existing PIC operates on per-token KV cache, yet linear-attention layers expose only a per-request recurrent state—leaving no per-token handle for *splice* or *correction*. The result is that most layers in a hybrid model lie outside the reach of existing PIC. No system today provides PIC for hybrid-attention LLMs.

We present HYPIC, the first serving system to deliver position-independent caching on hybrid-attention models. HYPIC rests on three contributions, each addressing a distinct obstacle that hybrid PIC raises and that no prior system solves.

**C1: A near-exact, constant-time state composition for linear-attention layers via cached transitions.** For linear-attention layers, the per-request recurrent state breaks the token-level *splice*-and-*correction* primitives that all prior PIC methods rely on, and naive end-state addition of each independent segment incurs non-negligible structural error. We identify the *segment-cumulative transition operator*—a fixed-size matrix that captures how the segment would transform any incoming recurrent state—as the missing algebraic primitive. Caching it alongside each segment’s zero-start end-state allows a near-exact, constant-time composition spanning all advanced linear-attention families. Since the operator depends only on tokens inside the segment, it can be computed once at first prefill and reused under any prefix.

**C2: Boundary-anchored alignment for the remaining full-attention layers via seam windows.** The minority full-attention layers in a hybrid stack still require PIC, but prior per-token *corrections* do not transfer directly. As shown in Fig. 1, linear layers break the per-token forward path: they retain only their end-states, blocking any non-final token from passing through the full-attention layers above. The two fallbacks—storing the per-token recurrent state at prohibitive storage cost, or forward-recurring from scratch for an arbitrarily selected token—are both unacceptable. We observe that under PIC *splice* in hybrid stacks, attention deviation concentrates sharply at both segment ends while interior positions stay largely unaffected. This locality lets HYPIC repair full-attention semantics by recomputing only a

small *seam window* anchored at each boundary, shrinking the recompute range from the segment length to a small constant.

**C3: Cache-miss acceleration for long cold requests via segment parallelism.** Cache misses are unavoidable, and long cold requests dominate tail TTFT. Existing PIC systems still prefill all cold segments on one instance sequentially, yet PIC itself has, in fact, already granted each segment self-containment—each segment can be prefilled from its own tokens independently. Yet no system to date has exploited this property to parallelize prefill across instances. HYPIC *dispatches* cache-miss segments of a single request to a worker pool in parallel, and a *combine* node then assembles the per-segment outputs into the request’s running state. HYPIC schedules segments under a Longest-Processing-Time-first (LPT) policy to balance load across workers, and pipelines each worker’s computation with transfer to minimize the *combine* node’s wait. This collapses tail TTFT severalfold, turning long cold requests into an accelerable workload.

We implement HYPIC on SGLang [53] and evaluate it across four hybrid-attention models on four public datasets and one production RAG trace. Against prefix caching—the production deployment baseline on hybrid models—HYPIC reduces TTFT by 2.45 $\times$  on average and improves peak throughput by 2.0 $\times$  at the same SLO, while staying within 3.3 points of full-recompute task accuracy. On cold-only requests, where prefix caching and prior PIC degrade to serial prefill, HYPIC delivers a 6.1 $\times$  TTFT speedup at 8 workers, removing long cold requests as a tail-latency contributor.

## 2 Background

### 2.1 Context Caching

To amortize prefill cost on long-context workloads, modern LLM serving systems adopt *context caching*, which reduces TTFT by reusing the attention intermediates of repeated tokens across requests. Existing approaches fall into two categories by reuse pattern: *position-dependent caching* (PDC) and *position-independent caching* (PIC).

**Position-dependent caching.** Modern transformers compute each token’s output as a softmax-weighted sum over its query against all preceding  $(k, v)$  pairs [35]. Once produced, these per-token tensors are immutable and can be materialized as a *KV cache* that grows linearly with context length. Modern serving systems [8, 16, 19, 50, 53] reuse this cache across requests via strict-prefix matching: when a new request shares its first  $n$  tokens with an earlier one, the first  $n$  KV entries can be reused directly. This is *position-dependent*—each  $(k, v)$  is jointly determined by token id and absolute position, and strict-prefix matching pins down both at once, so reuse is numerically exact. PDC therefore accelerates fixed system prompts and few-shot prefixes, but provides little

Family	Variant	$T_i$	$u_i$
Scalar	RetNet [32]	$\gamma I$	$k_i v_i^\top$
	Lightning-2 [28]	$\gamma I$	$k_i v_i^\top$
	Mamba2 [6]	$a_i I$	$k_i v_i^\top$
Diagonal	GLA [44]	$\text{diag}(g_i)$	$k_i v_i^\top$
Dense	DeltaNet [45]	$I - \beta_i k_i k_i^\top$	$\beta_i k_i v_i^\top$
	GDN [43]	$g_i (I - \beta_i k_i k_i^\top)$	$\beta_i k_i v_i^\top$
	KDA [18]	$(I - \beta_i k_i k_i^\top) \text{diag}(g_i)$	$\beta_i k_i v_i^\top$

**Table 1.** Unified parameterization of advanced linear-attention variants.  $k_i \in \mathbb{R}^{d_k}$  and  $v_i \in \mathbb{R}^{d_v}$  are the per-token key and value projections.  $\gamma$  is a per-head constant decay rate;  $a_i \in \mathbb{R}$ ,  $g_i \in \mathbb{R}^{d_k}$ , and  $\beta_i \in \mathbb{R}$  are data-dependent scalar, diagonal, and scalar gates produced from the input.

benefit for RAG and agentic workloads, where the same segment appears at different positions across requests and any prefix mismatch invalidates everything that follows [48].

**Position-independent caching.** A growing body of PIC work [3, 5, 12, 22–24, 36–38, 40–42, 48, 49, 52, 55] relaxes the strict-prefix constraint, allowing each semantically independent segment to be reused at arbitrary positions and behind arbitrary prefixes. The challenge is that a cached segment’s KV is bound to its original position and upstream context, so naive concatenation introduces numerical deviation. Most PIC work centers on selecting which tokens to recompute after splicing to suppress this deviation—e.g., CacheBlend [48] and CacheSlide [22] select the most-deviated tokens by KV deviation; ProphetKV [38], KVShare [41], and A<sup>3</sup> [55] locate critical tokens via attention distributions; CacheClip [40] relies on an auxiliary small model to predict recompute tokens. Despite the diversity of selection strategies, these methods all reduce to two sequential primitives: *splice*, which concatenates cached segments directly along the token axis, and *correction*, which adjusts positional encoding and recomputes a small set of tokens to restore contextual consistency.

## 2.2 Linear Attention

**Naive linear attention.** Katharopoulos et al. [17] replace the softmax kernel  $\exp(q^\top k / \sqrt{d})$  with a decomposable feature inner product  $\phi(q)^\top \phi(k)$ , decoupling the historical summation from  $q_i$ , and obtain the token-level recurrence

$$\begin{aligned}
 S_i &= S_{i-1} + \phi(k_i) v_i^\top, \\
 z_i &= z_{i-1} + \phi(k_i), \\
 o_i &= \frac{\phi(q_i)^\top S_i}{\phi(q_i)^\top z_i}.
 \end{aligned} \tag{1}$$

This reduces attention compute complexity from  $O(L^2 d)$  to  $O(L d^2)$ , and simultaneously compresses the cache from a growing per-token KV tensor to two fixed-size states—an associative memory matrix  $S \in \mathbb{R}^{d_k \times d_v}$  and a normalizer  $z \in \mathbb{R}^{d_k}$ .

$\ \Delta\ /\ S_{C_1 0}\ $	$ C_2 =256$	$ C_2 =512$	$ C_2 =1024$
$\gamma = 1 - 2^{-5}$	1.000	1.000	1.000
$\gamma = 1 - 2^{-7}$	0.866	0.982	1.000
$\gamma = 1 - 2^{-10}$	0.221	0.394	0.632

**Table 2.** Normalized naive-addition error  $\|\Delta\|/\|S_{C_1|0}\|$  for RetNet at varying decay  $\gamma$  and suffix length  $|C_2|$ .

**Advanced linear attention.** To improve model expressiveness, modern variants [6, 18, 28, 32, 43–45] introduce decay, gating, and delta erasure, dropping both the normalization denominator  $z$  and the explicit similarity kernel. Their token-level recurrence admits a unified form

$$\begin{aligned}
 S_i &= T_i S_{i-1} + u_i, \\
 o_i &= q_i^\top S_i,
 \end{aligned} \tag{2}$$

where  $T_i \in \mathbb{R}^{d_k \times d_k}$  is the transition operator and  $u_i \in \mathbb{R}^{d_k \times d_v}$  is the write term. Unlike  $S_i$ , which carries information forward,  $T_i$  and  $u_i$  are computed at every step from the current input and never persisted. By the form of  $T_i$ , existing variants fall into three families (Table 1): the first keeps  $T_i$  a scalar multiple of the identity (RetNet [32], Lightning-2 [28], Mamba2 [6]); the second relaxes it to a data-dependent diagonal (GLA [44]); the third stacks a low-rank outer-product term  $I - \beta_i k_i k_i^\top$  on top, enabling targeted directional erasure (DeltaNet [45], GDN [43], KDA [18]). The form of Equation (2) has been adopted by several recent production hybrid attention models (e.g., MiniMax-M1 [4], Jamba [20], Qwen3.5 [29], and Ring-2.5 [33]), which replace most full-attention layers with linear attention to bound per-token cost on long contexts. On Qwen3.5-35B-A3B [29], 30 of 40 layers are linear: each holds a fixed  $\sim 2$  MB of state per request, against  $\sim 256$  MB of KV cache for each full-attention layer at 128k context—over  $100\times$  smaller per layer.

## 3 Motivation

Hybrid-attention models are entering production (§2.2), yet all existing PIC systems target pure full-attention stacks (§2.1). Our goal is to build an efficient PIC system for hybrid-attention LLM serving; achieving this, however, is non-trivial: (i) Full-attention PIC primitives operate on per-token KV cache and do not transfer to the per-request recurrent state (§3.1). (ii) Full-attention layers in a hybrid stack cannot be corrected by existing PIC methods directly, which require per-token hidden states that linear layers suppress (§3.2). (iii) Long cold requests dominate tail latency, yet existing PIC systems still treat cold-segment prefill as sequential, missing the parallelism that segment self-containment enables (§3.3).

### 3.1 Existing PIC primitives do not transfer to linear-attention states

Naive full-attention PIC *splices* the KV caches of two segments along the token axis. Analogously, the most direct

linear-attention counterpart is to sum the end-states  $S_{C_1|0}$  and  $S_{C_2|0}$  of segments  $C_1$  and  $C_2$  (each computed from a zero initial state). Under naive linear attention (Equation (1)), this holds exactly. Initializing from  $S_{C_1|0}$  and unrolling the recurrence over  $C_2$  token-by-token gives

$$S_{C_1C_2|0} = S_{C_1|0} + S_{C_2|0}. \quad (3)$$

Since  $S_{C_2|0}$  accumulates only writes from  $C_2$ , it is independent of the starting state.

However, naive addition does not hold for advanced linear attention. Unrolling Equation (2) from  $S_{C_1|0}$  through the end of  $C_2$ , the true end-state is

$$S_{C_1C_2|0} = T_{C_2} S_{C_1|0} + S_{C_2|0}, \quad (4)$$

where  $T_C := \prod_{t \in C} T_t$  is the *segment-cumulative transition operator* of segment  $C$ . Naive addition omits  $T_{C_2}$ , and the error is

$$\Delta = \left( \prod_{t \in C_2} T_t - I \right) S_{C_1|0}. \quad (5)$$

This omission is structural rather than incidental. As noted in §2.2,  $T_i$  is computed at every step and never persisted, so any cache built on  $S_{C|0}$  alone cannot supply  $T_C$  at splice time, leaving naive addition—and the structural error of Equation (5)—as the only recourse. Taking the const-decay linear-attention (RetNet [32], Lightning-2 [28]) as an example, the error is  $\|\Delta\| = (1 - \gamma^{|C_2|}) \|S_{C_1|0}\|$ , jointly determined by decay coefficient  $\gamma$  and segment length  $|C_2|$ . Table 2 reports normalized error for RetNet. The slowest-decaying head ( $\gamma = 1 - 2^{-10}$ ) already reaches  $\|\Delta\| = 0.22 \|S_{C_1|0}\|$  at 256 tokens, and the fastest ( $\gamma = 1 - 2^{-5}$ ) saturates at  $\|\Delta\| = \|S_{C_1|0}\|$  at every segment length. Both far exceed any acceptable approximation. The gate and delta-rule families share this failure mode, as  $T_{C_2}$  does not collapse to the identity for any segment of positive length.

This failure, however, exposes an exploitable algebraic structure. Crucially, the *segment-cumulative transition operator*  $T_{C_2}$  is fully determined by tokens inside  $C_2$  and independent of the prefix state  $S_{C_1|0}$ — $T_i$  is computed solely from the current token’s decay coefficients, gating values, and other token-local features (Table 1), decoupled from the history  $S_{<i}$ . Likewise,  $S_{C_2|0}$ —the *zero-start end-state* of  $C_2$ —depends only on tokens inside  $C_2$ . Both quantities are independent of  $C_1$ —the algebraic basis for linear-attention PIC.

**Insight 1.** Linear-attention PIC admits a layer-exact and constant-time state composition. Both  $T_{C_2}$  and  $S_{C_2|0}$  are fully determined by tokens inside  $C_2$ , independent of the prefix. Left-multiplying  $S_{C_1|0}$  by  $T_{C_2}$  and adding  $S_{C_2|0}$  recovers the exact end-state of  $C_1C_2$ , eliminating the structural error of naive addition.

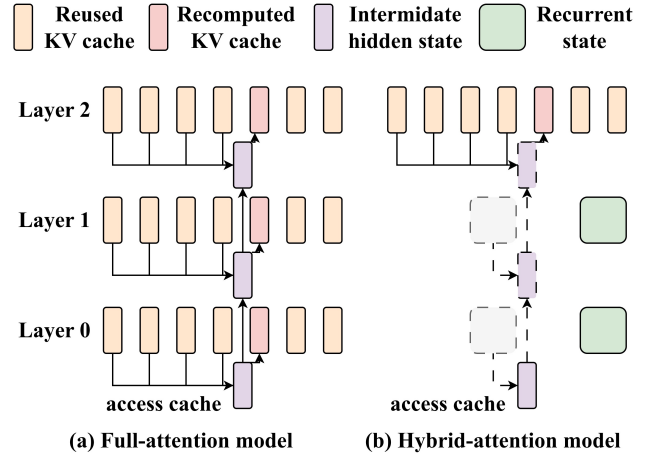


**Figure 2.** Memory-access footprint of *correction*. (a) Full-attention stack: every token’s prefix state is in the KV cache, so correction can read it directly. (b) Hybrid stack: linear layers retain only the per-request recurrent state, leaving non-final tokens’ prefix states uncached.

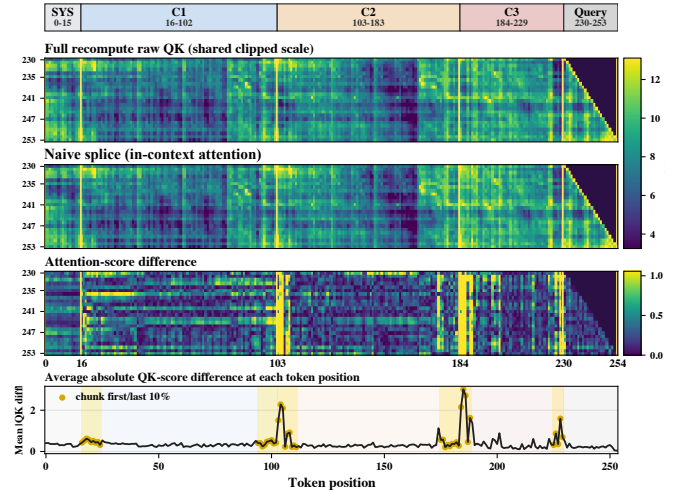


**Figure 3.** Attention-score deviation between Full Recompute and Naive Splice at Qwen3.5-35B-A3B layer 3, head 2. Deviation concentrates at segment boundaries while interior positions are largely unaffected.

### 3.2 Existing PIC primitives do not compose across hybrid stacks

In pure full-attention models, the *correction* primitive of PIC is well-validated: selecting a small number of tokens by deviation or attention weight and recomputing their  $(k, v)$  pairs restores full-attention semantics across segments after *splice*. Full-attention layers are a minority in a hybrid stack (25% of layers in Qwen3.5-35B-A3B) yet carry cross-segment look-back. Porting existing full-attention PIC *correction* to those layers is therefore the most direct approach.

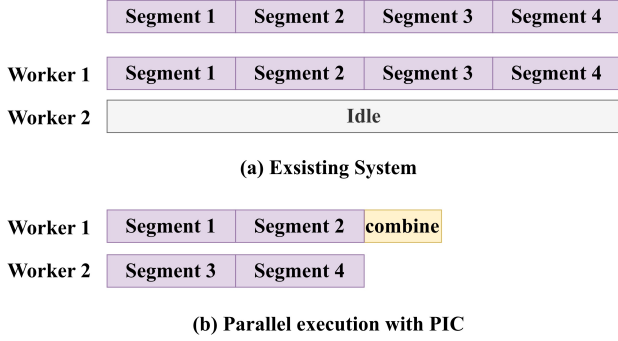


**Figure 4.** (a) Cache-miss prefill under PDC and existing PIC vs. (b) Parallel execution enabled by segment self-containment.

However, this migration assumes a prerequisite that does not hold in a hybrid stack. As shown in Fig. 2, recomputing  $(k_i^{(L)}, v_i^{(L)})$  at full-attention layer  $L$  for token  $i$  requires a single-token forward pass from layer 1 to  $L$ , which at each layer depends on the KV cache of the preceding  $i - 1$  tokens and token  $i$ 's own input hidden state. In a pure full-attention model, both are available—the KV cache is fully cached at prefill and the per-token hidden state is computed online at negligible cost. In a hybrid stack, linear layers store only the per-request recurrent state, blocking non-final tokens from passing through the full-attention layers above. Obtaining it to continue token  $i$ 's forward pass leaves only two options: (a) store per-token recurrent states during prefill—each token requires  $S_i^{(\ell)} \in \mathbb{R}^{d_k \times d_v}$ , which is  $d_k d_v / (d_k + d_v)$  times larger than full-attention KV ( $64 \times$  at  $d_k = d_v = 128$ ), not only erasing linear attention's storage advantage but also inflating total overhead; or (b) forward-recurse from the zero initial state—obtaining  $S_{i-1}^{(\ell)}$  requires  $i - 1$  recurrence steps from  $S_0$ , so recomputing a single token degrades to re-running all preceding tokens, eliminating the caching benefit entirely. Neither option is acceptable.

We therefore ask: is the ability to recompute an *arbitrary* token truly necessary? We compare full-attention scores at layer 3, head 2 of Qwen3.5-35B-A3B for all query tokens across segments under two conditions: Full Recompute, which sees the complete cross-segment context, and Naive Splice, which splices KV caches from segments prefilled independently. As shown in Fig. 3, deviation concentrates heavily at segment boundaries while interior positions exhibit far lower deviation. The head-side deviation is due to the intra-segment attention sink, consistent with prior observations in pure full-attention stacks [12, 39] and, as we show, persisting in hybrid stacks. The tail-side deviation is, to our knowledge, not previously characterized:  $C_n$ 's tail tokens are the natural targets of cross-segment lookback from  $C_{n+1}$ 's head tokens, yet  $C_{n+1}$  is prefilled in isolation and its query representations carry no cross-segment context from  $C_n$ ; at splice time, these context-blind queries produce distorted attention over  $C_n$ 's

tail, concentrating the deviation there. This locality shows that the *correction* scope does not need to range over the entire segment—a small constant window anchored at each boundary suffices.

**Insight 2.** Deviation in full-attention layers concentrates at head and tail boundaries, not the interior. Recomputing only a small window at each boundary therefore suffices—eliminating the need for per-token state storage or full-segment recurrence.

### 3.3 Existing PIC systems do not exploit segment-level self-containment

In RAG and agentic workloads, cache hits presuppose that a segment has been seen before, yet cache misses are unavoidable in practice—document corpora update continuously, and low-frequency documents are evicted under cache capacity limits. To accelerate long prefills, current serving systems apply *intra-instance* parallelism as the standard acceleration approach: tensor parallelism (TP) splits matrix operations across devices, and sequence parallelism (SP) distributes tokens within a single forward pass. Yet these strategies offer diminishing returns at scale. On our 8×H20 node (NVLink, 900 GB/s per GPU), prefilling a 100k-token request on Qwen3.5-35B-A3B takes 45.34 s with TP-1 and still 17.74 s with TP-8, far beyond interactive SLO.

The bottleneck is architectural. For a request containing  $n$  cold segments of  $|C|$  tokens each, PDC can only prefill the entire prompt sequentially due to causal dependency, with TTFT growing as  $O(n \cdot |C|)$ . *Intra-instance* parallelism strategies accelerate this pass but are confined to a single instance and cannot scale out efficiently. Existing PIC systems follow the same practice as PDC—prefilling all cold segments of a request on one instance sequentially, yielding the same  $O(n \cdot |C|)$  scaling. Long cold requests therefore remain the primary source of tail latency under both PDC and existing PIC systems.

In fact, PIC has already granted each segment self-containment: its prefill result is determined solely by its internal tokens, independent of other segments. This self-containment is precisely what licenses *inter-instance* parallel execution (Fig. 4)—dispatching  $n$  cold segments to  $m$  workers simultaneously and assembling the results at a combine node reduces TTFT from  $O(n \cdot |C|)$  to  $O(|C| + c)$ , where  $c$  is the bounded combine overhead. Yet no existing PIC system provides such a distributed cold-prefill mechanism.

**Insight 3.** PIC renders each segment's prefill self-contained—each segment can be prefilled from its own tokens independently. Cold segments of a single request can therefore be dispatched to separate workers in parallel, turning long cold requests from an  $O(n \cdot |C|)$  serial bottleneck into an  $O(|C| + c)$  parallelizable workload.

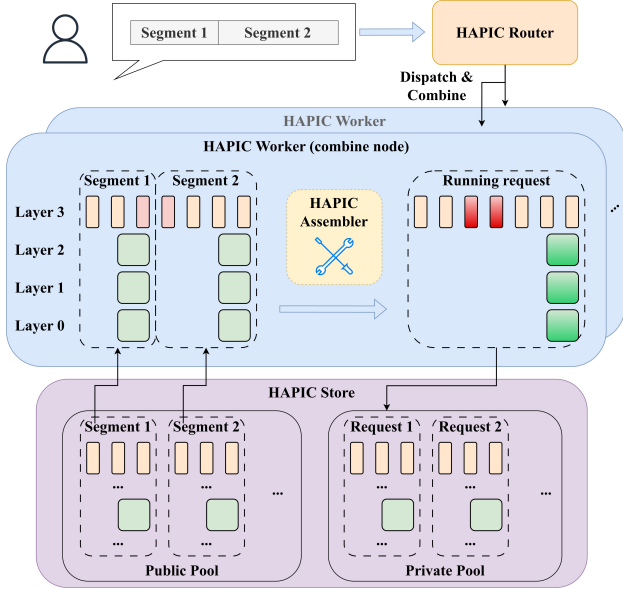


Figure 5. HYPIC architecture.

## 4 HYPIC Design

### 4.1 Overview

HYPIC consists of three core components: the *HYPIC Router*, the *HYPIC Store*, and the *HYPIC Assembler*. Fig. 5 shows the overall architecture and the end-to-end path of a single request. When a request arrives, the *HYPIC Router* splits it into a sequence of segments along application-provided segment boundaries (e.g., document separators in a RAG template, turn boundaries in an agent trace), and queries the *HYPIC Store* to determine each segment’s hit status. The router picks a *combine node* among idle inference nodes for this request, and dispatches the miss segments to multiple prefill workers in parallel. Each worker computes the *segment-cumulative transition operator* and the *zero-start end-state* for linear-attention layers, and the segment-local KV for full-attention layers (§4.4). Once all segments are ready, the *HYPIC Assembler* on the combine node reconstructs the request’s running state—composing per-segment states in constant time at linear-attention layers via the cached transitions (§4.2), and recomputing the seam window to repair attention-sink and cross-segment lookback at full-attention layers (§4.3).

The *HYPIC Store* is a per-node cache pool partitioned into a *public pool* and a *private pool*. The public pool holds segment-granularity linear-attention and full-attention cache, shared across requests and nodes. The private pool holds per-request assembled running state, used exclusively by the owning request’s decode phase.

### 4.2 State composition with cached transitions

**Cached transitions and composition law.** As described in §3.1, naive linear-attention PIC fails because it omits the

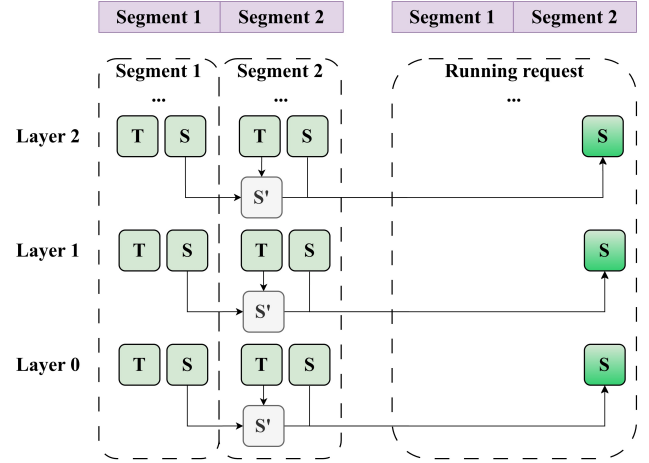


Figure 6. Linear-attention state composition with cached transitions. Each segment caches the tuple  $(T_C, S_{C|0})$  at first prefill; at reuse time HYPIC composes the prefix end-state and the cached tuples via Equation (6).

*segment-cumulative transition operator*—a quantity computed as a transient intermediate at every recurrence step yet never persisted by current serving systems. To address this, HYPIC caches not only the *zero-start end-state*  $S_{C|0}$  of segment  $C$ , but also the *segment-cumulative transition operator*  $T_C$  at first prefill, forming a binary cache tuple  $(T_C, S_{C|0})$  per segment. On a cache hit, HYPIC recomposes the cached tuple with the running state via the composition law in  $O(1)$  with respect to  $|C|$ —given a prefix end-state  $S_S$  and  $n$  suffix segments  $C_1, \dots, C_n$ , we have

$$S_{S C_1 \dots C_n} = \left( \prod_{i=n}^1 T_{C_i} \right) S_S + \sum_{i=1}^n \left( \prod_{j=n}^{i+1} T_{C_j} \right) S_{C_i|0}, \quad (6)$$

where  $\prod_{i=n}^1 T_{C_i} \triangleq T_{C_n} \dots T_{C_1}$ . Fig. 6 illustrates state composition with cached transitions for a two-segment example.

We further analyze the storage and compute overhead of  $T_C$ . As noted in §2.2, the transition operator  $T_i$  differs across model variants, so the compressibility of the segment-cumulative  $T_C$  varies accordingly. Table 3 lists the stored object and its cost for each variant. In terms of storage, for RetNet [32] and Lightning-2 [28],  $T_C = \gamma^{|C|} I$  is a scalar multiple of the identity, so only the scalar  $\gamma^{|C|}$  need be cached. For GLA [44],  $T_C = \text{diag}(\prod_t g_t)$  remains diagonal and can be compressed to the diagonal vector  $\prod_t g_t \in \mathbb{R}^{d_k}$ . DeltaNet [45], GDN [43], and KDA [18] introduce a low-rank outer-product term  $I - \beta k k^\top$ —the iterated product no longer remains sparse and must be cached as a dense matrix  $\in \mathbb{R}^{d_k \times d_k}$ . In terms of compute, applying  $T_C$  to an existing state  $S$  costs  $O(d_k d_v)$  for scalar and diagonal families, as both reduce to element-wise scaling of  $S \in \mathbb{R}^{d_k \times d_v}$ . The dense family requires a full matrix-matrix multiply at  $O(d_k^2 d_v)$ , a modest increase but still independent of segment length  $|C|$ , as is the former.

Family	Variant	$T_C$ closed form	Stored as	Storage cost	Apply cost
Scalar	RetNet [32]	$\gamma^{ C }I$	$\gamma^{ C }$	4 B	$O(d_k d_v)$
	Lightning-2 [28]	$\gamma^{ C }I$	$\gamma^{ C }$	4 B	$O(d_k d_v)$
	Mamba2 [6]	$(\prod_t a_t)I$	$\prod_t a_t$	4 B	$O(d_k d_v)$
Diagonal	GLA [44]	$\text{diag}(\prod_t g_t)$	$\prod_t g_t \in \mathbb{R}^{d_k}$	256 B	$O(d_k d_v)$
Dense	DeltaNet [45]	$\prod_t (I - \beta_t k_t k_t^\top)$	$T_C \in \mathbb{R}^{d_k \times d_k}$	32 KB	$O(d_k^2 d_v)$
	GDN [43]	$(\prod_t g_t) \cdot \prod_t (I - \beta_t k_t k_t^\top)$	$T_C \in \mathbb{R}^{d_k \times d_k}$	32 KB	$O(d_k^2 d_v)$
	KDA [18]	$\prod_t [(I - \beta_t k_t k_t^\top) \text{diag}(g_t)]$	$T_C \in \mathbb{R}^{d_k \times d_k}$	32 KB	$O(d_k^2 d_v)$

**Table 3.** Per-segment  $T_C$  storage by variant, at  $d_k=d_v=128$ , fp16, per head per layer. Apply cost is the complexity of computing  $T_C \cdot S$  at splice time.

**State cache management.** As shown in Fig. 5, HYPIC partitions the cache into two independently managed pools, as the stored objects and their usage patterns differ fundamentally. The public pool stores the per-segment *zero-start end-state*  $S_{C|0}$  and the *segment-cumulative transition operator*  $T_C$ , which are both required for state composition and shared across requests. The private pool stores only the per-request *running state*—the fully composed state that incorporates all prefix information and drives the subsequent decode phase—without  $T_C$ , since composition is complete and decode reads only  $S$ . Each pool maintains an independent capacity budget and follows a Least-Recently-Used (LRU) eviction policy, ensuring hot cache remains resident in HBM while cold entries are reclaimed.

Private cache is exclusively owned by a single request, yet it is not released immediately after decode completes: in multi-turn dialogue and iterative agent calls, successive requests from the same session can reuse it directly via prefix caching. On new requests, HYPIC first looks up the private pool for a prefix hit, and then queries the public pool for PIC hits on the remaining segments. This design ensures that position-dependent and position-independent caching coexist as complementary reuse paths, rather than one supplanting the other.

**Causal convolution state warm-up.** Some models (e.g., Qwen3.5 [29]) prepend a causal conv1d to the QKV projection, requiring the preceding  $k-1$  tokens’ hidden states as input. HYPIC caches the trailing conv state alongside  $(T_C, S_{C|0})$  and excludes each segment’s leading  $k-1$  tokens from the  $T_C$  and  $S_{C|0}$  accumulation. At reuse time, the leading  $k-1$  tokens of  $C_i$  are recomputed with  $C_{i-1}$ ’s trailing tokens as conv input to warm up the conv state, then composed into the running state via Equation 6.

**State RoPE re-rotation.** Some models with a scalar transition operator (e.g., Ring-2.5 [33]) apply Rotary Position Embedding (RoPE) [31] to  $K$  inside the linear layer. Because  $T_i = \gamma I$  commutes with any rotation matrix, the RoPE property  $R(a+b) = R(a)R(b)$  yields, for any two start positions  $a$  and  $b$ , the exact relation

$$S_{C|b} = R(b-a) S_{C|a}. \quad (7)$$

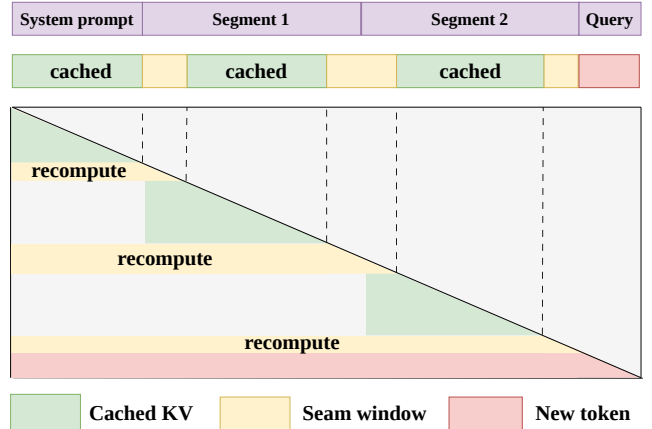


**Figure 7.** Seam window across adjacent segments ( $C_1, C_2$ ): the last  $w$  tokens of  $C_1$  and the first  $w$  tokens of  $C_2$  are excluded from each segment’s cached state and recomputed jointly at splice time.

At cache time, HYPIC stores the zero-start end-state  $S_{C|0}$  in the public pool. At reuse time, HYPIC replaces each  $S_{C|0}$  in Equation (6) with  $R(p_i) S_{C|0}$  before the prefix  $T$ -products act, where  $p_i$  is segment  $C_i$ ’s global start position in the spliced sequence.

**Fidelity analysis.** We measure the fidelity of HYPIC’s linear-attention composition on Qwen3.5-35B-A3B [29]. We split a 1096-token prompt into 4 segments, independently compute each segment’s zero-start end-state  $S_{C|0}$  and the segment-cumulative transition operator  $T_{C_i}$ , then compose the full-prompt running state via Equation (6). Compared against a single-pass full recompute, the composed state matches to  $6 \times 10^{-5}$  in relative norm and  $0.003^\circ$  in direction at layer 0—within only FP16 noise. Our composition law eliminates the structural error of naive addition, ensuring a layer-exact splice of independently cached states. We analyze the end-to-end fidelity across all layers in §6.3.

### 4.3 Full attention alignment with seam windows

**Seam window for recomputation.** As discussed in §3.2, full-attention PIC does not transfer directly to the hybrid

stack, while the concentration of attention deviation at segment boundaries opens an opportunity to restore cross-segment attention without heavy compute or storage. As shown in Fig. 7, for any adjacent segment pair  $(C_1, C_2)$ , HYPIC concatenates  $C_1$ 's last  $w$  tokens with  $C_2$ 's first  $w$  tokens into a contiguous small window, which we call the *seam window*.

At cache time, HYPIC runs full attention over every token in the segment but caches only the interior KV—the  $w$  tokens at each end are computed but not stored, since they are guaranteed to be recomputed at splice time independent of which neighbor the segment is later paired with. At splice time, the seam window accesses all cached KV through the causal mask, thereby repairing both the attention-sink and cross-segment lookback identified in §3.2. The two boundary segments of a request are handled specially. The leading segment is typically the system prompt, which has no left neighbor and always anchors at position 0, so no cross-segment deviation needs repair and HYPIC caches it in full without seam exclusion. The trailing segment is the user query, whose prefix varies per request and which must attend to every preceding token, so HYPIC recomputes it end-to-end rather than caching.

In practice  $w$  is small—we use  $w = 8$  as the default. Since segment lengths in compositional workloads are typically larger than 512 tokens, the seam covers only a negligible fraction of each segment and the recompute overhead is bounded. We confirm that this width is sufficient to keep task accuracy within an acceptable envelope in §6.4. Although Fig. 3 shows the head-side (attention-sink) and tail-side (cross-segment lookback) deviations differ in magnitude, both decay sharply within the same small range, so we apply a single symmetric  $w$  to cover both ends without separately tuned widths.

Supporting seam-window recompute also requires the linear-attention layers to forward-propagate individual seam tokens, not just the aggregated end-state—otherwise the full-attention layers above would have no per-token input hidden state to recompute the seam KV from. As shown in Fig. 8, HYPIC excludes the  $w$  tokens at each end of every segment from the  $T_C$  and  $S_{C|0}$  accumulation at cache time, and at splice time computes the seam window's own  $T$  and  $S$  on the fly, applying the composition law (Equation 6) to both advance the running state and emit each seam token's per-layer output for the next layer above. When the model also has a causal convolution (§4.2),  $w \geq k-1$  guarantees the seam recompute itself warms up the boundary conv state—the two mechanisms unify without additional cost.

**KV RoPE re-rotation and cache management.** Following prior PIC work [24, 37, 49, 55], HYPIC re-rotates  $K$  at splice time:  $V$  is RoPE-independent,  $Q$  is regenerated from the running hidden state, and the seam tokens are recomputed rather than retrieved, so only the cached interior  $K$  requires re-rotation. By  $R(a+b) = R(a)R(b)$ , moving a cached

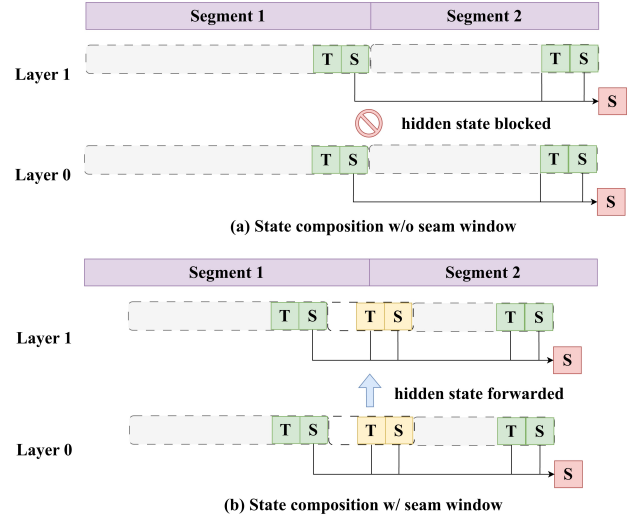


**Figure 8.** Seam-window handling at linear-attention layers. Each segment caches  $(T_C, S_{C|0})$  over interior tokens only; at splice time HYPIC recomputes the seam window's own  $T$  and  $S$  on the fly and inserts them into the composition law, jointly advancing the running state and forwarding per-token outputs to the layer above.

key from start  $a$  to start  $b$  reduces to one left-multiplication:

$$K_b = R(b-a) K_a. \quad (8)$$

These interior tokens are served from a two-pool layout: each segment caches its interior  $K$  under local (0-based) positions and  $V$  as-is in the public pool, making both reusable by any hitting request regardless of prefix; on a cache hit, HYPIC rotates the 0-based  $K$  to the segment's global position in the current request and writes the result into private slots for subsequent decoding. This per-request duplication of  $K$  is necessary rather than wasteful: the same cached segment hit by multiple concurrent requests sits at a different global position in each, so no single rotated copy can be shared—rotating on demand from the 0-based public copy is the only way to preserve cross-request reuse.

#### 4.4 Cache-miss acceleration with segment parallelism

**Two-phase segment parallelism.** As §3.3 established, PIC has already granted each segment self-containment, which licenses *inter-instance* parallelism on cold prefill—a lever neither PDC nor prior PIC systems have exploited, leaving long cold requests on the  $O(n \cdot |C|)$  serial path. HYPIC introduces *segment parallelism*, an inter-instance scheme scoped to the prefill stage that decomposes each cache-miss prefill into a two-phase task—*dispatch* and *combine* (Fig. 9).

In the *dispatch* phase, when a PIC request arrives, the router decomposes it, looks up each segment in the global cache index, and dispatches only the *cold* segments in parallel

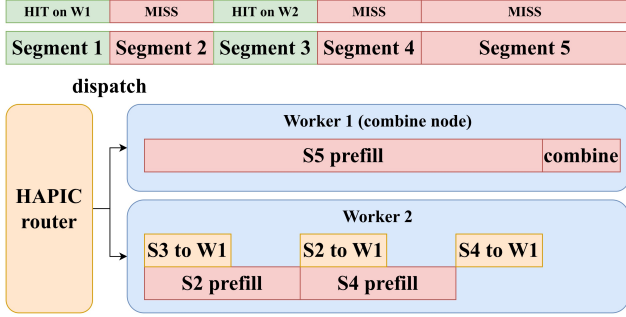


**Figure 9.** Accelerate long cold requests with segment parallelism. The HYPIC Router probes hit status for each segment (Seg 1, 3 hit; Seg 2, 4, 5 miss), LPT-dispatches the miss segments across the worker pool (Seg 2 and 4 to Worker 2; Seg 5 to Worker 3), and designates Worker 1 as the combine node, which pulls cache from peers and assembles the running state.

to a prefill worker pool—each worker prefills its segment from scratch, yielding the tuple  $(T_C, S_{C|0})$  together with the segment-local full-attention KV. In the *combine* phase, the combine node fetches hit-segment KV. In the *combine* phase, the combine node fetches hit-segment caches from peers holding a copy and collects the  $(T_C, S_{C|0})$  tuples together with full-attention KV streamed back from the dispatched workers, then composes the per-segment states into a single running state via the cached transitions (§4.2) and recomputes the seam-window tokens to repair full-attention alignment (§4.3). Once prefill completes, the assembled state is forwarded to the decode worker along the normal path.

On a worker pool of size  $m$ , cold-prefill TTFT drops from the prior  $O(n \cdot |C|)$  serial path to  $O(\lceil n/m \rceil \cdot |C| + c)$ , collapsing to  $O(|C| + c)$  when  $m \geq n$ , where  $c$  is the bounded combine-side cost—cross-node transfer, state composition, and seam recompute.

**Load-balance policy.** Since segment lengths are uneven, overall prefill latency is bounded by the slowest worker—a classical load-balancing problem over the cold subset. Let  $C = \{C_1, \dots, C_n\}$  be the cold segments of the request with token counts  $|C_i|$ , and  $\mathcal{W} = \{w_1, \dots, w_m\}$  the available workers. For an assignment  $a : C \rightarrow \mathcal{W}$ , HYPIC minimizes the heaviest worker’s token load:

$$\min_a \max_{w \in \mathcal{W}} \sum_{C_i: a(C_i)=w} |C_i|. \quad (9)$$

HYPIC solves this with the Longest Processing Time first (LPT) greedy: traverse  $C$  in descending order of  $|C_i|$  and assign each segment to the worker with the smallest accumulated token count.

**Pipelining computation and transfer.** Default serving stacks batch co-located requests to maximize compute utilization, but the same batching habit applied to segment parallelism would have each worker ship its segments only

after the last one finishes, leaving the combine node stalled on a synchronized burst. HYPIC instead finalizes one segment at a time and issues its transfer immediately, overlapping it with the next segment’s compute. For sufficiently large segments ( $\geq 1024$  tokens), per-segment dispatch preserves kernel efficiency while flattening the transfer burst.

**Orthogonality to intra-instance parallelism.** *Inter-instance* parallelism partitions a request across instances with PIC, while *intra-instance* parallelism accelerates the forward pass within a single instance. The two levers act on disjoint axes and compose without modification: each instance still runs under its intra-instance parallel configuration, and inter-instance parallelism only changes how the router assigns segments across instances. A request with  $n$  cold segments served on an  $m$ -worker pool of TP- $t$  instances therefore enjoys both effects multiplicatively—segment dispatch shortens the critical path from  $O(n \cdot |C|)$  to  $O(\lceil n/m \rceil \cdot |C| + c)$ , while TP- $t$  further reduces each per-segment prefill. Segment parallelism is most useful when intra-instance parallelism has saturated; otherwise the router degenerates to placing the entire request on one worker, incurring no additional cost over the baseline serving path.

## 5 Implementation

We implement HYPIC on SGLang [53] with 14k lines of Python and Triton code. As illustrated in Fig. 5, our implementation comprises three key components: the *HYPIC Router*, the *HYPIC Store*, and the *HYPIC Assembler*.

**Serving interfaces.** Following prior work [48], HYPIC treats any request containing the PIC\_SEPARATOR marker as PIC-enabled and uses the marker to delimit segments. `split_and_tokenize(text, separator)` splits the prompt and tokenizes each segment independently, and `match(req)` hashes each segment by its token ids and returns the matched cache entries. To warm up a segment for future requests, applications simply issue it wrapped between two PIC\_SEPARATOR markers—the segment is then resident in the serving instance and immediately available for reuse.

**Router and store.** HYPIC realizes the dispatch path of §4.4 by extending `sglang_router` with a segment-level hit-status probe and an LPT assigner, and transports both peer-pulled hit caches and worker-streamed miss outputs over SGLang’s existing KV-transfer layer (RDMA [10]/NCCL [25] P2P). The combine node pre-allocates slots for every segment of the request up front and ships the slot handles to the assigned workers, so each worker’s  $(T_C, S_{C|0})$  tuple and segment-local KV land directly. Each worker overlaps segment  $i+1$ ’s prefill with segment  $i$ ’s transfer on a separate copy CUDA stream, gated by a per-segment CUDA event.

**Assembler.** HYPIC derives both  $S_{C|0}$  and  $T_C$  from the same recurrence  $S_i = T_i S_{i-1} + u_i$  by invoking the FLA [46] kernel

twice on the miss-segment batch. The first invocation yields  $S_{C|0}$  with  $S_0=0$ , while the second yields  $T_C$  with  $S_0=I$  and  $u_t$  zeroed, since  $(\prod_t T_t) I = T_C$ .

## 6 Evaluation

### 6.1 Setup

**Hardware.** We run all experiments on a node with 8×NVIDIA H20-3e GPUs, each with 141 GB HBM and fully connected by 18-link NVLink, dual-socket Intel Xeon 6759P-C totaling 120 physical cores, 2 TB DDR5 DRAM, and six Mellanox ConnectX RDMA NICs at 200 Gbps HDR and 400 Gbps NDR.

**Models.** We evaluate four production hybrid-attention model configurations spanning both ends of Tab. 3: Ring-mini-linear-2.0 and Ring-flash-linear-2.0 [33], whose linear layers use scalar decay, and Qwen3.5-35B-A3B and Qwen3.5-122B-A10B [29], whose linear layers use a dense matrix transition.

**Workloads.** We evaluate HYPIC on four public datasets and one production trace: **(W1) HotpotQA** [47] and **(W2) TriviaQA** [15], multi-hop and open-domain QA where each prompt concatenates retrieved evidence passages; **(W3) MultiNews** [7] and **(W4) GovReport** [13], multi-document summarization with long segments and high per-prompt segment count; and **(W5) Prod-RAG**, a production RAG trace from a major content platform that retrieves user-published notes to answer search queries (mean input 12k tokens), with bursty arrivals and heavy-tailed note popularity.

**Methods.** We compare four methods that bracket the design space: (i) **Full Recompute** [53]: no cache reuse; every prompt is prefilled from scratch—the upper bound on accuracy and the lower bound on speed. (ii) **Prefix Cache** [53]: standard PDC; reuses strict prefix matches only—what production systems run today on hybrid models. (iii) **Naive Addition**: the most direct PIC strawman for the hybrid stack; caches per-segment  $S_{C|0}$  alone (without  $T_C$ ) and reuses by addition, with no full-attention KV recompute—the structural lower bound on fidelity for any hybrid-attention PIC. (iv) **HYPIC**: our full system, which composes cached linear-attention states with the segment-accumulated transition operator and recomputes an 8-token seam window at each segment boundary.

**Metrics.** We use the following metrics to evaluate serving performance and task accuracy. (i) **TTFT** measures the interval from request arrival to the first response token, capturing the user-perceived responsiveness of the service. (ii) **Throughput** is the processed tokens per second per GPU, capturing the aggregate serving capacity of the cluster. (iii) **ROUGE-L** [21] is the longest-common-subsequence overlap between the model output and the reference, used on the summarization workloads (W3, W4). Higher values indicate

more reference content preserved. (iv) **F1** [30] is the token-level harmonic mean of precision and recall between the predicted and gold answer, used on the QA workloads (W1, W2). It ranges from 0 to 1 and penalizes both missing and spurious tokens.

### 6.2 End-to-end performance

**Accuracy–TTFT Pareto.** We first validate that HYPIC reduces TTFT with minimal quality loss. Fig. 10 plots task accuracy against p50 TTFT across four model configurations and four datasets. Across the 16 model–dataset cells, HYPIC reduces p50 TTFT by 2.46× over Full Recompute and 2.43× over Prefix Cache on average, with a maximum 8.6× reduction on Qwen3.5-122B MultiNews. Ring models show smaller relative speedups because their Full Recompute baseline is already short, but HYPIC still moves Ring-mini by 1.37× and Ring-flash by 2.04× on average. The average task-score loss is small: HYPIC drops only 1.36 points on Qwen3.5 and 5.31 points on Ring, averaging 3.34 points across all 16 cells, while Naive Addition loses 25.3 score points on average. Prefix Cache yields little speedup because its strict-prefix matching rarely fires on RAG-shaped inputs, confirming PDC’s brittleness on this workload class. In a few cells Prefix Cache even reports TTFT above Full Recompute; this stems from an implementation artifact in upstream SGLang and is orthogonal to our design.

**TTFT and throughput under load.** We next characterize HYPIC’s latency and throughput on a real RAG workload. We replay the Prod-RAG trace, rescaling original arrivals to evaluate at various QPS levels. Fig. 11 reports p50 TTFT and peak per-GPU token throughput against QPS. On the TTFT–QPS curve, at a common TTFT SLO of 1 s, HYPIC raises the sustainable QPS by 1.28× (1.38×, 2.83×, 2.16×) over Prefix Cache and by 1.33× (1.47×, 3.00×, 2.20×) over Full Recompute on Ring-mini (Ring-flash, Qwen3.5-35B, Qwen3.5-122B), respectively. On the throughput–QPS curve, Prefix Cache saturates cluster compute at 12 (5, 3, 2) QPS on Ring-mini (Ring-flash, Qwen3.5-35B, Qwen3.5-122B), where token throughput peaks—HYPIC pushes this saturation knee out to 20 (10, 10, 4) QPS and lifts the saturated throughput by 1.24× (1.30×, 2.11×, 1.72×) over Prefix Cache.

### 6.3 Linear-attention state composition

We further examine Equation (6) in §4.2 along two axes: (i) its scalability with context length and segment count, and (ii) its deep-layer fidelity after the composed state propagates through every linear-attention layer.

**Scalability of state composition.** Here, we use two sweeps to verify the scalability of state composition. We first fix the number of segments at 4 and vary per-segment length from 1k to 4k tokens, yielding total prompt lengths from roughly 4k to 16k tokens. As shown in Fig. 12(a), Full

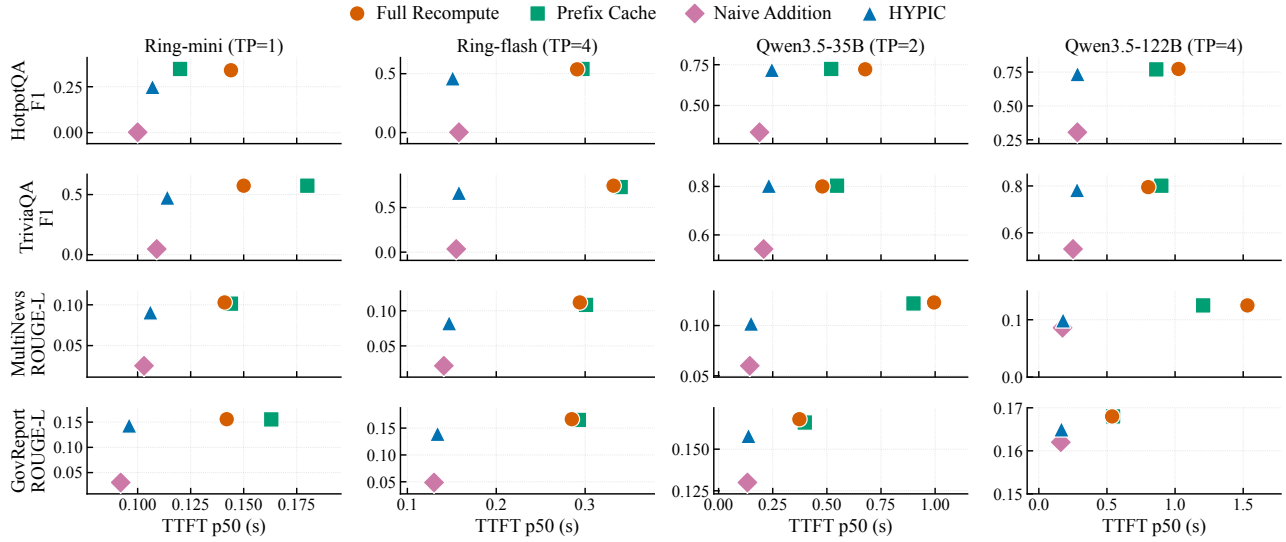


Figure 10. Accuracy–TTFT Pareto across four models and four datasets.

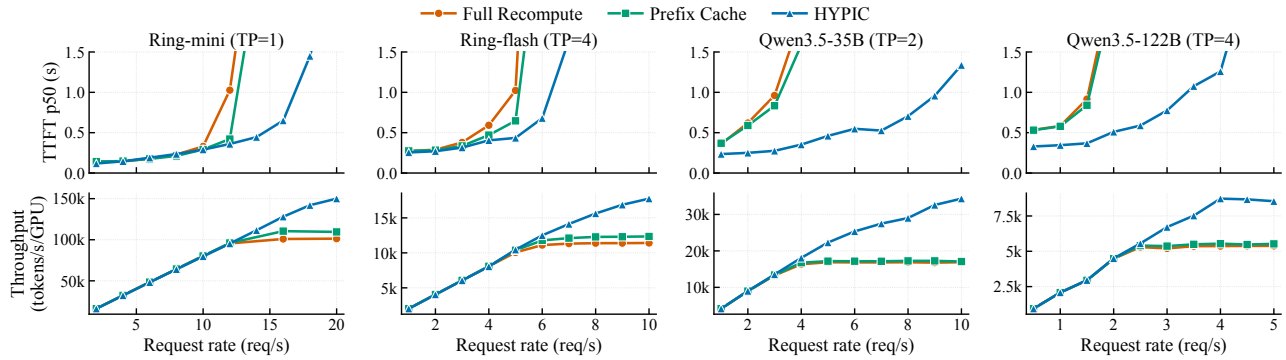


Figure 11. P50 TTFT and per-GPU token throughput at various QPS on the Prod-RAG trace.

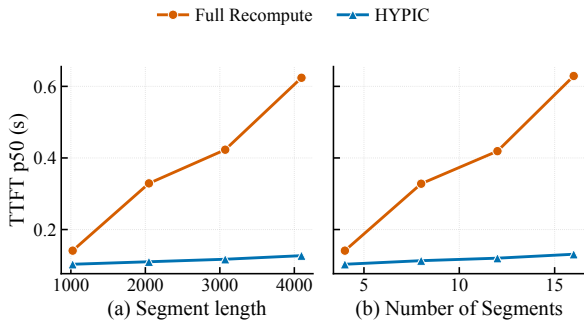


Figure 12. Linear-attention composition scaling: accuracy and TTFT against (a) per-segment length at a fixed segment count of 4, and (b) segment count at a fixed per-segment length of 1k tokens.

Recompute grows from 0.141 s to 0.624 s as the prompt becomes 4× longer, while HYPIC grows only from 0.103 s to

0.127 s—a speedup that rises from 1.37× at 4k tokens to 4.91× at 16k tokens.

We next vary the number of retrieved segments  $n$  from 4 to 16 at a fixed 1k tokens per segment. Fig. 12(b) shows that HYPIC incurs an incremental cost of only 2.3 ms per additional segment, compared with 40.7 ms for Full Recompute, reaching a 4.80× TTFT speedup at the largest point. HYPIC’s TTFT grows only marginally across both sweeps, as composition is  $O(n)$  in segment count and independent of per-segment length  $|C|$ .

**Deep-layer fidelity.** HYPIC’s state composition is algebraically exact given the same input hidden state (§4.2), yet deeper layers may still drift, since their inputs differ between intra-segment prefill and full-prompt prefill. We therefore measure the error at the deepest linear layer between HYPIC and Full Recompute with a controlled 512-token, two-chunk prompt on Qwen3.5-35B-A3B and Ring-flash. To isolate this effect from full attention, we skip all full-attention layers in this experiment so that the hidden state propagates only through linear layers, with all other logic unchanged—we

Model	Relative $L_2$	Angular error
Qwen3.5-35B-A3B	8.92%	5.11°
Ring-flash	8.69%	4.98°

**Table 4.** Deep-layer state drift of HYPIC vs. Full Recompute at the deepest linear layer, after the composed state propagates through all linear-attention layers.

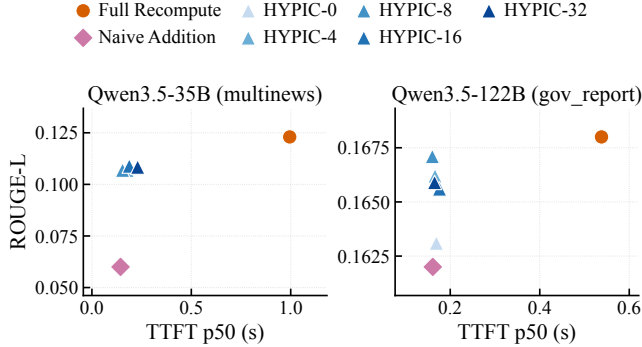


**Figure 13.** Task accuracy and TTFT against window width  $w$  per segment boundary.

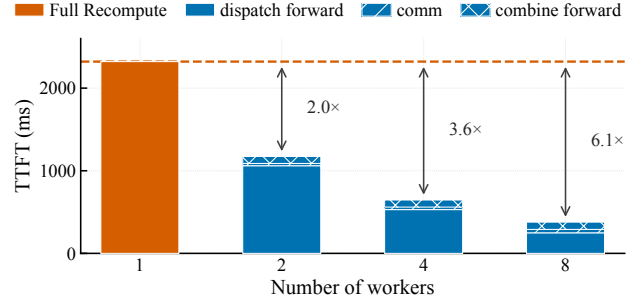
compute per-segment end-states and transitions independently, compose the running state via Equation (6), and compare it against Full Recompute.

Table 4 reports the results. For Qwen3.5-35B-A3B, the composed state differs from Full Recompute by 8.92% in relative  $L_2$  and 5.11° in direction. Ring-flash gives 8.69% and 4.98° under the same metric. Both models stay within a 10% state-drift envelope after propagating through all linear-attention layers, matching the small task-score losses in Fig. 10.

The residual drift is not a defect of Equation (6), which is exact given any input and removes the structural error of Naive Addition. Rather, it arises from the inputs themselves, as isolated per-segment prefill strips out the cross-segment context that Full Recompute carries in each  $C_k$ 's hidden state—a limitation shared by all prior PIC systems [12, 38, 48]. The cached  $(T_C, S_{C|0})$  tuple is therefore exact only at layer 0 and degrades to an approximation above, with drift that amplifies with depth but stays within a controlled range—a cost we accept for  $O(1)$  reuse over per-prefix recomputation.

#### 6.4 Seam window for full-attention alignment

**Sensitivity of seam window width.** We sweep  $w \in \{0, 4, 8, 16, 32\}$  to (i) characterize how accuracy and TTFT vary with seam width and (ii) validate the default  $w=8$  used in §6.2. The sweep is run on two cells: Qwen3.5-122B on GovReport and Qwen3.5-35B on MultiNews. As shown in Fig. 13, for Qwen3.5-122B on GovReport, a small seam window recovers most of the boundary error—ROUGE-L improves from 0.1631 at  $w=0$  to 0.1671 at  $w=8$ , close to the Full Recompute score of 0.168. For Qwen3.5-35B on MultiNews, enlarging  $w$



**Figure 14.** Segment parallelism TTFT breakdown into dispatch forward (parallel per-segment prefill), comm (cross-node KV pull), and combine forward (state composition and seam recompute) as we sweep prefill worker count  $n$ .

from 8 to 32 raises TTFT by 76 ms while ROUGE-L varies within 0.15 points. Thus,  $w=8$  suffices as the default.

#### 6.5 Segment parallelism for cache-miss prefill

**Segment parallelism TTFT breakdown.** Here we evaluate the scalability of segment parallelism and break down its TTFT. The workload is an 11-segment prompt of 2.4k tokens per segment with every segment forced to miss, and we sweep the prefill worker count  $n \in \{1, 2, 4, 8\}$ . Full Recompute processes the entire prompt serially, while HYPIC dispatches the  $n$  segment prefills in parallel and then assembles the request at the combine node.

Fig. 14 decomposes HYPIC's TTFT into *dispatch forward* (parallel per-segment prefill), *comm* (cross-node KV pull), and *combine forward* (state composition and seam recompute). Full Recompute takes 2321 ms on a single instance, while HYPIC reduces TTFT to 1173 ms, 646 ms, and 378 ms at  $n=2, 4$ , and 8 via segment parallelism, corresponding to 2.0×, 3.6×, and 6.1× speedups. The dispatch forward falls from 1061 ms at  $n=2$  to 530 ms at  $n=4$  and 249 ms at  $n=8$ , matching the expected parallel-prefill scaling. In contrast, communication stays small at 27–41 ms and combine remains nearly flat at 85–88 ms, showing that state composition and seam recompute do not become the new bottleneck. This validates that segment parallelism reduces cache-miss prefill from  $O(n \cdot |C|)$  to  $O(\lceil n/m \rceil \cdot |C| + c)$ —scalability follows the available worker count, while KV transfer and combine-node assembly stay bounded by a small constant independent of prompt length.

## 7 Conclusion

HYPIC is the first serving system to deliver position-independent caching on hybrid-attention LLMs. It caches a segment-cumulative transition operator to compose linear-attention states in constant time, repairs full-attention layers with a small boundary seam window, and parallelizes

cold prefill across workers by exploiting segment self-containment. Across four hybrid-attention models and five workloads, HYPIC reduces TTFT by 2.45× and improves peak throughput by up to 2.0× over existing systems at the same SLO, stays within 3.3 points of full-recompute accuracy, and delivers a 6.1× cold-prefill speedup at 8 workers.

## References

- [1] Amey Agrawal, Nitin Kedia, Ashish Panwar, Jayashree Mohan, Nipun Kwatra, Bhargav Gulavani, Alexey Tumanov, and Ramachandran Ramjee. 2024. Taming Throughput-Latency Tradeoff in LLM Inference with Sarathi-Serve. In *18th USENIX Symposium on Operating Systems Design and Implementation (OSDI '24)*. USENIX Association, 117–134.
- [2] Yushi Bai, Xin Lv, Jiajie Zhang, Hongchang Lyu, Jiankai Tang, Zhidian Huang, Zhengxiao Du, Xiao Liu, Aohan Zeng, Lei Hou, et al. 2024. LongBench: A Bilingual, Multitask Benchmark for Long Context Understanding. In *Proceedings of the 62nd Annual Meeting of the Association for Computational Linguistics*. 3119–3137.
- [3] Ziyi Cao, Qingsi Si, Jingbin Zhang, and Bingquan Liu. 2026. Sparse Attention Across Multiple-Context KV Cache. In *Proceedings of the AAAI Conference on Artificial Intelligence*, Vol. 40. 30165–30173. doi:10.1609/aaai.v40i36.40266
- [4] Aili Chen, Aonian Li, Bangwei Gong, Binyang Jiang, Bo Fei, Bo Yang, Boji Shan, Changqing Yu, Chao Wang, Cheng Zhu, et al. 2025. MiniMax-M1: Scaling Test-Time Compute Efficiently with Lightning Attention. *arXiv preprint arXiv:2506.13585*.
- [5] Chuangtao Chen, Grace Li Zhang, Xunzhao Yin, Cheng Zhuo, Bing Li, and Ulf Schlichtmann. 2026. KV Packet: Recomputation-Free Context-Independent KV Caching for LLMs. *arXiv:2604.13226 [cs.CL]*
- [6] Tri Dao and Albert Gu. 2024. Transformers are SSMs: Generalized Models and Efficient Algorithms Through Structured State Space Duality. In *Proceedings of the 41st International Conference on Machine Learning (Proceedings of Machine Learning Research, Vol. 235)*. PMLR, 10041–10071.
- [7] Alexander Richard Fabbri, Irene Li, Tianwei She, Suyi Li, and Dragomir Radev. 2019. Multi-News: A Large-Scale Multi-Document Summarization Dataset and Abstractive Hierarchical Model. In *Proceedings of the 57th Annual Meeting of the Association for Computational Linguistics*. 1074–1084.
- [8] In Gim, Guojun Chen, Seung-Seob Lee, Nikhil Sarda, Anurag Khandelwal, and Lin Zhong. 2024. Prompt Cache: Modular Attention Reuse for Low-Latency Inference. In *Proceedings of Machine Learning and Systems*, Vol. 6.
- [9] Bogdan Gliwa, Iwona Mochol, Maciej Biesek, and Aleksander Wawer. 2019. SAMSum Corpus: A Human-Annotated Dialogue Dataset for Abstractive Summarization. In *Proceedings of the 2nd Workshop on New Frontiers in Summarization (EMNLP-IJCNLP 2019 Workshop)*. 70–79.
- [10] Chuanxiong Guo, Haitao Wu, Zhong Deng, Gaurav Soni, Jianxi Ye, Jitendra Padhye, and Marina Lipshteyn. 2016. RDMA over Commodity Ethernet at Scale. In *Proceedings of the ACM SIGCOMM Conference*. 202–215. doi:10.1145/2934872.2934908
- [11] Xanh Ho, Anh-Khoa Duong Nguyen, Saku Sugawara, and Akiko Aizawa. 2020. Constructing a Multi-hop QA Dataset for Comprehensive Evaluation of Reasoning Steps. In *Proceedings of the 28th International Conference on Computational Linguistics*. 6609–6625.
- [12] Junhao Hu, Wenrui Huang, Weidong Wang, Haoyi Wang, Tiancheng Hu, Qin Zhang, Hao Feng, Xusheng Chen, Yizhou Shan, and Tao Xie. 2025. EPIC: Efficient Position-Independent Caching for Serving Large Language Models. In *Proceedings of the 42nd International Conference on Machine Learning (Proceedings of Machine Learning Research, Vol. 267)*. PMLR, 24391–24402.
- [13] Luyang Huang, Shuyang Cao, Nikolaus Parulian, Heng Ji, and Lu Wang. 2021. Efficient Attentions for Long Document Summarization. In *Proceedings of the 2021 Conference of the North American Chapter of the Association for Computational Linguistics*. 1419–1436.
- [14] Carlos E Jimenez, John Yang, Alexander Wettig, Shunyu Yao, Kexin Pei, Ofir Press, and Karthik Narasimhan. 2024. Swe-bench: Can language models resolve real-world github issues?. In *International Conference on Learning Representations*, Vol. 2024. 54107–54157.
- [15] Mandar Joshi, Eunsol Choi, Daniel S. Weld, and Luke Zettlemoyer. 2017. TriviaQA: A Large Scale Distantly Supervised Challenge Dataset for Reading Comprehension. In *Proceedings of the 55th Annual Meeting of the Association for Computational Linguistics*, Vol. 1. 1601–1611.
- [16] Jordan Juravsky, Bradley Brown, Ryan Ehrlich, Daniel Y. Fu, Christopher Ré, and Azalia Mirhoseini. 2024. Hydragen: High-Throughput LLM Inference with Shared Prefixes. In *Proceedings of the 41st International Conference on Machine Learning (ICML '24)*.
- [17] Angelos Katharopoulos, Apoorv Vyas, Nikolaos Pappas, and François Fleuret. 2020. Transformers are RNNs: Fast Autoregressive Transformers with Linear Attention. In *Proceedings of the 37th International Conference on Machine Learning (ICML)*.
- [18] Kimi Team. 2025. Kimi Linear: An Expressive, Efficient Attention Architecture. *arXiv:2510.26692 [cs.CL]* <https://arxiv.org/abs/2510.26692>
- [19] Woosuk Kwon, Zhuohan Li, Siyuan Zhuang, Ying Sheng, Lianmin Zheng, Cody Hao Yu, Joseph E. Gonzalez, Hao Zhang, and Ion Stoica. 2023. Efficient Memory Management for Large Language Model Serving with PagedAttention. In *Proceedings of the 29th ACM Symposium on Operating Systems Principles (SOSP '23)*. ACM, 611–626.
- [20] Opher Lieber, Barak Lenz, Hofit Bata, Gal Cohen, Jhonathan Osin, Itay Dalmedigos, Erez Safahi, Shaked Meirum, Yonatan Belinkov, Shai Shalev-Shwartz, et al. 2024. Jamba: A hybrid transformer-mamba language model. *arXiv preprint arXiv:2403.19887 (2024)*.
- [21] Chin-Yew Lin. 2004. ROUGE: A Package for Automatic Evaluation of Summaries. In *Text Summarization Branches Out*. 74–81.
- [22] Yang Liu, Yunfei Gu, Liqiang Zhang, Chentao Wu, Guangtao Xue, Jie Li, Minyi Guo, Junhao Hu, and Jie Meng. 2026. CacheSlide: Unlocking Cross Position-Aware KV Cache Reuse for Accelerating LLM Serving. In *Proceedings of the 24th USENIX Conference on File and Storage Technologies (FAST '26)*. USENIX Association, 83–99.
- [23] Songshuo Lu, Hua Wang, Yutian Rong, Zhi Chen, and Yaohua Tang. 2025. TurboRAG: Accelerating Retrieval-Augmented Generation with Precomputed KV Caches for Chunked Text. In *Proceedings of the 2025 Conference on Empirical Methods in Natural Language Processing*. Association for Computational Linguistics, 6588–6601. doi:10.18653/v1/2025.emnlp-main.334
- [24] Dongyang Ma, Yan Wang, and Tian Lan. 2025. Block-Attention for Efficient Prefilling. In *The Thirteenth International Conference on Learning Representations*.
- [25] NVIDIA. 2024. *NCCL: NVIDIA Collective Communications Library*. <https://github.com/NVIDIA/nccl>
- [26] Pratyush Patel, Esha Choukse, Chaojie Zhang, Aashaka Shah, Íñigo Goiri, Saeed Maleki, and Ricardo Bianchini. 2024. Splitwise: Efficient Generative LLM Inference Using Phase Splitting. In *Proceedings of the 51st Annual International Symposium on Computer Architecture (ISCA '24)*. IEEE, 118–132.
- [27] Ruoyu Qin, Zheming Li, Weiran He, Jialei Cui, Feng Ren, Mingxing Zhang, Yongwei Wu, Weimin Zheng, and Xinran Xu. 2025. Mooncake: Trading More Storage for Less Computation – A KVCache-Centric Architecture for Serving LLM Chatbot. In *23rd USENIX Conference on File and Storage Technologies (FAST '25)*. USENIX Association.
- [28] Zhen Qin, Weigao Sun, Dong Li, Xuyang Shen, Weixuan Sun, and Yiran Zhong. 2024. Lightning Attention-2: A Free Lunch for Handling Unlimited Sequence Lengths in Large Language Models. *arXiv:2401.04658 [cs.CL]*
- [29] Qwen Team. 2026. Qwen3.5: Towards Native Multimodal Agents. Qwen Technical Blog. <https://qwen.ai/blog?id=qwen3.5>

- [30] Pranav Rajpurkar, Jian Zhang, Konstantin Lopyrev, and Percy Liang. 2016. SQuAD: 100,000+ Questions for Machine Comprehension of Text. In *Proceedings of the 2016 Conference on Empirical Methods in Natural Language Processing*. 2383–2392.
- [31] Jianlin Su, Yu Lu, Shengfeng Pan, Ahmed Murtadha, Bo Wen, and Yunfeng Liu. 2024. RoFormer: Enhanced Transformer with Rotary Position Embedding. *Neurocomputing* 568 (2024), 127063.
- [32] Yutao Sun, Li Dong, Shaohan Huang, Shuming Ma, Yuqing Xia, Jilong Xue, Jianyong Wang, and Furu Wei. 2023. Retentive Network: A Successor to Transformer for Large Language Models. arXiv:2307.08621 [cs.CL]
- [33] Ling Team, Bin Han, Caizhi Tang, Chen Liang, Donghao Zhang, Fan Yuan, Feng Zhu, Jie Gao, Jingyu Hu, Longfei Li, et al. 2025. Every attention matters: An efficient hybrid architecture for long-context reasoning. *arXiv preprint arXiv:2510.19338* (2025).
- [34] Harsh Trivedi, Niranjan Balasubramanian, Tushar Khot, and Ashish Sabharwal. 2022. MuSiQue: Multihop Questions via Single-hop Question Composition. *Transactions of the Association for Computational Linguistics* 10 (2022), 539–554.
- [35] Ashish Vaswani, Noam Shazeer, Niki Parmar, Jakob Uszkoreit, Llion Jones, Aidan N. Gomez, Lukasz Kaiser, and Illia Polosukhin. 2017. Attention Is All You Need. In *Advances in Neural Information Processing Systems*, Vol. 30.
- [36] Jiahao Wang, Weiyou Xie, Mingxing Zhang, Boxing Zhang, Jianwei Dong, Yuening Zhu, Chen Lin, Jinqi Tang, Yaochen Han, Zhiyuan Ai, Xianglin Chen, Yongwei Wu, and Congfeng Jiang. 2026. From Prefix Cache to Fusion RAG Cache: Accelerating LLM Inference in Retrieval-Augmented Generation. *Proceedings of the ACM on Management of Data* 4, 1 (2026). doi:10.1145/3786655
- [37] Qian Wang, Zahra Yousefjamarani, Morgan Lindsay Heisler, Rongzhi Gu, Xiaolong Bai, Yizhou Shan, Wei Zhang, Lan Wang, Ying Xiong, Yong Zhang, and Zhenan Fan. 2025. MEPIC: Memory Efficient Position Independent Caching for LLM Serving. arXiv:2512.16822 [cs.LG]
- [38] Shihao Wang, Jiahao Chen, Yanqi Pan, Hao Huang, Yichen Hao, Xianguyu Zou, Wen Xia, Wentao Zhang, Chongyang Qiu, and Pengfei Wang. 2026. ProphetKV: User-Query-Driven Selective Recomputation for Efficient KV Cache Reuse in Retrieval-Augmented Generation. arXiv:2602.02579 [cs.AI]
- [39] Guangxuan Xiao, Yuandong Tian, Beidi Chen, Song Han, and Mike Lewis. 2024. Efficient Streaming Language Models with Attention Sinks. In *The Twelfth International Conference on Learning Representations*.
- [40] Bin Yang, Qiuyu Leng, Jun Zeng, and Zhenhua Wu. 2025. CacheClip: Accelerating RAG with Effective KV Cache Reuse. arXiv:2510.10129 [cs.LG]
- [41] Huan Yang, Renji Zhang, Mingzhe Huang, Weijun Wang, Yin Tang, Yuanchun Li, Yunxin Liu, and Deyu Zhang. 2025. KVShare: An LLM Service System with Efficient and Effective Multi-Tenant KV Cache Reuse. arXiv:2503.16525 [cs.LG]
- [42] Jingbo Yang, Bairu Hou, Wei Wei, Yujia Bao, and Shiyu Chang. 2025. KVLink: Accelerating Large Language Models via Efficient KV Cache Reuse. In *Advances in Neural Information Processing Systems*, Vol. 38.
- [43] Songlin Yang, Jan Kautz, and Ali Hatamizadeh. 2025. Gated Delta Networks: Improving Mamba2 with Delta Rule. In *The Thirteenth International Conference on Learning Representations*.
- [44] Songlin Yang, Bailin Wang, Yikang Shen, Rameswar Panda, and Yoon Kim. 2024. Gated Linear Attention Transformers with Hardware-Efficient Training. In *Proceedings of the 41st International Conference on Machine Learning (Proceedings of Machine Learning Research, Vol. 235)*. PMLR, 56501–56523.
- [45] Songlin Yang, Bailin Wang, Yu Zhang, Yikang Shen, and Yoon Kim. 2024. Parallelizing Linear Transformers with the Delta Rule over Sequence Length. In *Advances in Neural Information Processing Systems*, Vol. 37.
- [46] Songlin Yang and Yu Zhang. 2024. FLA: A Triton-Based Library for Hardware-Efficient Implementations of Linear Attention Mechanism. <https://github.com/fla-org/flash-linear-attention>
- [47] Zhilin Yang, Peng Qi, Saizheng Zhang, Yoshua Bengio, William W. Cohen, Ruslan Salakhutdinov, and Christopher D. Manning. 2018. HotpotQA: A Dataset for Diverse, Explainable Multi-hop Question Answering. In *Proceedings of the 2018 Conference on Empirical Methods in Natural Language Processing*. 2369–2380.
- [48] Jiayi Yao, Hanchen Li, Yuhao Liu, Siddhant Ray, Yihua Cheng, Qizheng Zhang, Kuntai Du, Shan Lu, and Junchen Jiang. 2025. CacheBlend: Fast Large Language Model Serving for RAG with Cached Knowledge Fusion. In *Proceedings of the Twentieth European Conference on Computer Systems (EuroSys '25)*. ACM. doi:10.1145/3689031.3696098
- [49] Hancheng Ye, Zhengqi Gao, Mingyuan Ma, Qinsi Wang, Yuzhe Fu, Ming-Yu Chung, Yueqian Lin, Zhijian Liu, Jianyi Zhang, Danyang Zhuo, and Yiran Chen. 2025. KVCOMM: Online Cross-context KV Cache Communication for Efficient LLM-based Multi-agent Systems. In *Advances in Neural Information Processing Systems*.
- [50] Lu Ye, Ze Tao, Yong Huang, and Yang Li. 2024. ChunkAttention: Efficient Self-Attention with Prefix-Aware KV Cache and Two-Phase Partition. In *Proceedings of the 62nd Annual Meeting of the Association for Computational Linguistics*. 11608–11620.
- [51] Qingfei Zhao, Ruobing Wang, Yukuo Cen, Daren Zha, Shicheng Tan, Yuxiao Dong, and Jie Tang. 2024. LongRAG: A Dual-Perspective Retrieval-Augmented Generation Paradigm for Long-Context Question Answering. In *Proceedings of the 2024 Conference on Empirical Methods in Natural Language Processing*. 22600–22632.
- [52] Shiju Zhao, Junhao Hu, Jiaqi Zheng, and Guihai Chen. 2026. You Need an Encoder for Native Position-Independent Caching. arXiv:2602.01519 [cs.CL] <https://arxiv.org/abs/2602.01519>
- [53] Lianmin Zheng, Liangsheng Yin, Zhiqiang Xie, Jeff Huang, Chuyue Sun, Cody Hao Yu, Shiyi Cao, Christos Kozyrakis, Ion Stoica, Joseph E. Gonzalez, Clark Barrett, and Ying Sheng. 2024. SGLang: Efficient Execution of Structured Language Model Programs. In *Advances in Neural Information Processing Systems*.
- [54] Yinmin Zhong, Shengyu Liu, Junda Chen, Jianbo Hu, Yibo Zhu, Xuanzhe Liu, Xin Jin, and Hao Zhang. 2024. DistServe: Disaggregating Prefill and Decoding for Goodput-Optimized Large Language Model Serving. In *18th USENIX Symposium on Operating Systems Design and Implementation (OSDI '24)*. USENIX Association, 193–210.
- [55] Yuechi Zhou, Yi Su, Jianxin Zhang, Juntao Li, Qingrong Xia, Zhefeng Wang, Xinyu Duan, and Baoxing Huai. 2025. A3: Attention-Aware Accurate KV Cache Fusion for Fast Large Language Model Serving. arXiv:2511.17560 [cs.CL]